Asian Journal of Chemistry; Vol. 38, No. 5 (2026), 1245-1252

ASIAN JOURNAL OF CHEMISTRY

https://doi.org/10.14233/ajchem.2026.35579

Macroalgae Aquatic Weed *Azolla pinnata* Biochar: Production and Characterisation

B. SINGHA[1] and D. DEKA[2,*]

[1]Department of Chemistry, Gauhati University, Guwahati-781001, India
[2]Department of Chemistry, Mizoram University, Aizawl-796004, India

*Corresponding author: E-mail: dcdeka@gauhati.ac.in

Received: 8 January 2026 *Accepted*: 23 March 2026 *Published online*: 4 May 2026 AJC-22349

In this study, the spectroscopic and physico-chemical properties of biochar derived from waste biomass of aquatic plant *Azolla pinnata* are reported. The biochar produced by pyrolysis at 500 ºC was characterised by PXRD, XRF, FESEM, EDX, BET, FTIR and TGA analysis. The biochar is basic in nature, contains mesopores and diverse nanoparticles that exhibit irregular shapes and sizes. It has strong thermal stability with moderate surface area which increases by 31.71% after pyrolysis. Spectroscopic and chemical analyses indicate that the primary constituents of the biochar are KCl, NaCl and SiO_2, along with significant amounts of MgO, CaO and $CaCO_3$. It has features similar to other Ca-rich waste biomass-derived catalysts utilised in transesterification processes, making it a viable candidate heterogeneous base catalyst for organic reactions. Furthermore, due to its high concentration of beneficial nutrient combinations such as Ca, Mg, N, P and K, it is a potential natural fertilizer to boost agricultural productivity as well as a natural cure for acidic soil.

Keywords: *Azolla pinnata*, Aquatic weeds, Biochar, Macroalgae, Waste to wealth.

INTRODUCTION

Aquatic plants easily inhabit lakes and polluted waters, have attracted considerable interest from researchers to investigate their potential applications owing to their rapid growth rates, high biomass production and ease of maintenance and harvesting. One such unique aquatic plant that can reproduce and double its biomass in just two days is *Azolla*. *Azolla* is a miniature and fast-growing aquatic fern which grows in stagnant water bodies such as ponds and lakes and is found all over Asia, Africa and America. The fern has a symbiotic association with a nitrogen fixing cyanobiont *Anabaena Azollae* [1]. The endosymbiont provides sufficient nitrogen for both itself and its host [2]. This symbiotic association helps it to reproduce at a very fast rate.

The term Azolla is a combination of two Greek words 'azo' and 'allyo' which means 'to dry' and 'to kill' respectively, implying that the plant dies as it dries. It was initially coined by French scientist Jean Bapitiste Lamarck in 1783 [3]. Lamarck classified the genus Azolla as belonging to the division Polypodiophyta, class Polypodiopsida, order Salviniales and family Salviniaceae [3]. The genus has six surviving species: *Azolla filiculoides*, *Azolla microphylla*, *Azolla caroliniana*, *Azolla mexicana*, *Azolla pinnata* and *Azolla nilotica* all of which are globally distributed throughout the world. *Azolla pinnata* is widespread across Asia and along the tropical African coast.

Aquatic plants are the foundation of a water body's health and productivity and are vital components of natural aquatic systems. Conversely, excessive growth of aquatic vegetation necessitates management as it turns into noxious aquatic weeds in nutrient-rich habitats. The excessive proliferation of *Azolla* creates dense mats over water bodies, diminishing dissolved oxygen levels and endangering aquatic creatures. The unchecked proliferation of aquatic plants competes with other aquatic species for resources such as light, oxygen and nutrients and may contaminate water bodies upon decomposition [4]. By obstructing the drainage systems, they also prevent water from flowing freely in irrigation structures, alter the soil's salinity and alkalinity and contaminate the surrounding area by choking. Thus, to ensure the survival of aquatic species and maintain the ecosystem and health of the water body, it is essential to eradicate the excessive proliferation of aquatic plants. This can be done by utilizing the waste biomass of aquatic plants in a variety of applications.

Waste biomass derived applications have recently grown in importance as people look for sustainable and eco-friendly methods, particularly in the light of the current world situation, which includes population explosion, global warming and strict pollution rules. Preserving and restoration of ecosystems associated to water, such as lakes, wetlands, aquifers and rivers is one of the 17 Sustainable Development Goals (SDGs) of the 2030 Agenda for Sustainable Development, which was adopted by all United Nations Member States in 2015. Utilizing such aquatic plant waste biomass in a range of research domains can help achieve this goal by transforming biowaste to biowealth. Biomass obtained from *Azolla* has been applied in a variety of research fields such as using the biomass in wastewater treatment [5,6], phytoremediation of different contaminants such as heavy metals [7], as a biofertilizer [8], CO_2 sequestration [9], increasing soil fertility [10], animal feed [11], as a space food [12], *etc*. Thus, it is evident that *Azolla* has demonstrated its potential in a variety of applications, ranging from biofertilizer to space food. In a study of *Azolla*, Wagner refers to it as "a green gold mine" because of its many applications [13]. However, there is no literature currently available on the study of its biochar.

Biochar is a carbon-rich, cost-effective material which is derived from a variety of waste biomass and has a wide range of applications [14,15]. Although there are many basic uses for biochar, the most popular reported ones are improving nutrient interactions in soil to increase fertility and productivity [16] and immobilizing different pollutants in soil for soil remediation [17]. Other applications of biochar include adsorbing carcinogenic organic dyes like indigo carmine [18], effectively eliminating organic pollutants [19] and toxic heavy metals like lead and mercury from wastewater systems [20]. Moreover, biochar serves as a resilient carbon sink capable of remaining in the soil for over a century, garnering significant interest from both the scientific community and the public as an innovative approach to carbon capture and storage (CCS). In this context, the utilisation of waste-biomass-derived biochar catalysts in numerous organic reactions has recently gained tremendous importance due to their low cost and widespread availability while also making the process ecofriendly and greener [21,22]. Waste biomass derived heterogeneous catalyst such as waste egg shells [23], waste oyster shell [24], *etc*. have been successfully applied as a catalyst in numerous organic reactions thus making the process eco-friendly as well as mitigating the problem of solid waste disposal.

Therefore, in this paper, we report the physico-chemical properties and spectroscopic characterization of *Azolla pinnata* biochar as well as investigate its biochar as a potential candidate heterogeneous base catalyst in the future, based on its spectroscopic and physico-chemical characterisation and by comparing the results to other reported biomass-based biochar catalysts. This work therefore offers baseline data that allows evaluation of the spectroscopic and physico-chemical characteristics as well as its possibility to be used as a potential candidate heterogeneous base catalyst in future.

EXPERIMENTAL

Sample collection and preparation of *Azolla pinnata* biochar: *A. pinnata* (Fig. 1) is abundantly available throughout Northeast India. It is found as a free-floating water fern in various lakes and ponds. Samples were collected from the freshwater lake Deepor beel, located at 26.13ºN 91.66ºE, Assam, India. It is a natural wetland of significant biological and environmental significance that has a wide variety of plants and animals and designated as a Ramsar Site. Various free-floating, underwater and emergent aquatic macrophytes are found throughout the year in this lake, with their abundance increasing during the rainy season. These include *Eicchornia crassipes*, *Azolla pinnata*, *Pistia stratiotes*, *Lemna minor*, *Lemna major* and *Spirodela polyrrhiza*.

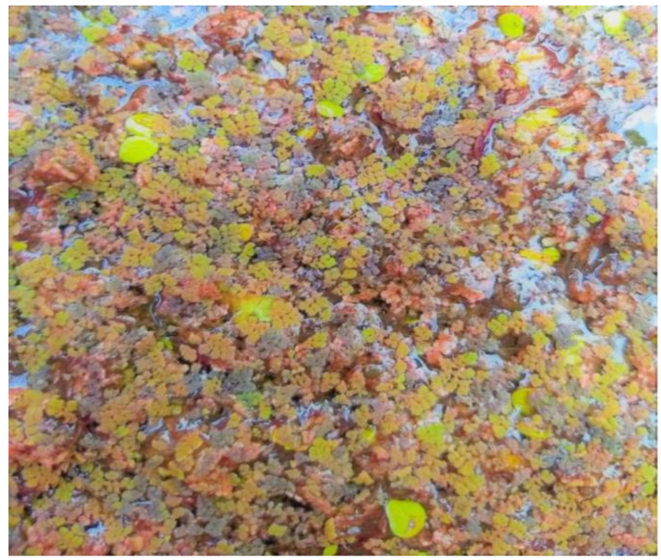

Fig. 1. Image of thick mat of *A. pinnata* from Deepor Beel Wetland, Assam, India

The *Azolla pinnata* biomass was washed thoroughly with fresh water to remove impurities and air-dried for several days, reducing 3 kg of wet mass to 250 g of dry material. The dried sample was slowly burned in an earthen tray to obtain 31 g of ash, which was cooled and ground to obtain a homogeneous powder, designated as APA-C0. This material was further calcined at 500 ºC for 3 h in a muffle furnace to produce biochar (APA-C500). The resulting biochar was cooled in a desiccator to room temperature and stored for further use.

Physico-chemical properties

Moisture content, loss on ignition, ash content and pH: Moisture content, loss on ignition and ash content were done according to ASTM D7348-08. The pH of the water extract of the biomass was measured according to ASTM D1293A. Before all the tests were performed, conditioning of new silica crucibles was done by heating under the conditions of the test and then cooling it before use. The moisture content was determined by heating 0.5 g of dry ash (APA-C0) in the preconditioned crucible at 110 ºC for 2 h in a muffle furnace and weighed after cooling down to ambient temperature in a desiccator. It was calculated using eqn. 1:

$$M = \frac{W_i - W_f}{W_i} \times 100 \quad (1)$$

where M = percent moisture as determined in the test specimen, W_i = initial mass of test specimen used, g, W_f = mass of test specimen after drying in moisture test, g.

The loss on ignition (LOI) was determined using a single-step procedure. A new preheated and cooled silica crucible was taken and 0.2 g of the sample was weighed. The crucible with the sample was placed into the cold furnace without a cover with air as furnace atmosphere. The furnace's temperature was increased gradually until the furnace reached 450-500 ºC after 1 h and 750 ºC after 2 h. The temperature was kept stable for an extra 2 h. It was calculated using eqn. 2:

$$\mathrm{LOI} = \frac{W_i - W_f}{W_i} \times 100 \qquad (2)$$

where W_i = mass of test specimen used and W_f = mass of test specimen after heating at 750 ºC.

Similarly, to determine the ash content, a silica crucible was pre-conditioned and cooled before weighing 0.2 g of sample. The crucible containing the sample was placed in the cold furnace without a cover, with air as the furnace environment. The temperature of the furnace was gradually increased until it reached 450-500 ºC after 1 h and 750 ºC after 2 h. An additional 2 h were spent maintaining the temperature. It was calculated using eqn. 3:

$$\text{Ash content (A)} = \frac{W_f}{W_i} \times 100 \qquad (3)$$

where W_i = mass of test specimen used and W_f = mass of ash residue after heating at 750 ºC.

BET surface area, pore volume and pore size: BET Micromeritics Tristar 3000 equipment was used to measure the surface area, pore volume and pore size. Adsorption of N_2 adsorption-desorption isotherms at 77 K were used to calculate the specific surface area using the Brunauer-Emmett-Teller (BET) formula. Nitrogen adsorption data were collected over a relative pressure (P/P_0) range of 0.05-0.30. The samples were degassed for 3 h at 50-250 ºC in a helium atmosphere before being subjected to N_2 adsorption analysis. The Barrett-Joyner-Halenda (BJH) technique was used to determine pore size distributions from desorption isotherms.

Characterization: Thermal stability of the uncalcined *A. pinnata* sample (APA-C0) was analysed by TGA (TGA/DSC-1, METTLER TOLEDO) from ambient temperature to 700 ºC at 10 ºC min^{-1} under nitrogen. Functional groups of APA-C0 and calcined biochar (APA-C500) were identified using FT-IR (Shimadzu AFFINITY-1) in the range 4000-400 cm^{-1}. Surface morphology and elemental composition were examined by FESEM coupled with EDX after gold coating. Crystalline phases were analysed using PXRD (Rigaku Ultima-IV, Cu*K*α radiation, 2θ = 10-80º) and elemental oxide composition was determined by XRF (Zetium X-ray fluorescence spectrometer). The pH was measured using a digital pH meter (Eutech Instrument, pH 510, pH/mV/ºC) at room temperature (24 ºC). The calibration of the instrument was done using buffer having pH 4, pH 7 and pH 10.

RESULTS AND DISCUSSION

Moisture content, loss on ignition, ash content and pH: Table-1 shows that APA-C0 possesses a moisture content of 15.58%, indicating the presence of physically adsorbed water associated with the porous biomass structure. The loss on ignition (49.63%) at 750 ºC reflects the substantial removal of volatile matter and decomposition of organic constituents. As presented in Table-2, the ash content was 50.36%, suggesting a high proportion of inorganic mineral components in the sample. The aqueous suspension exhibited a pH of 10.54, confirming the basic nature of APA-C0, which can be attributed to the presence of alkaline mineral oxides and carbonates.

BET surface area, pore volume and pore size: From the BET surface area, pore volume and pore size measurement it was found that the BET surface area of the uncalcined *A. pinnata* biochar (APA-C0) is 8 m^2/g with corresponding micropore volumes 0.0077 cm^3/g (Table-3). The (APA-C0) contains mesopores (2-50 nm). The pore size value 16.2 nm indicates relatively narrow pore size distribution. The BET surface area of the calcined *A. pinnata* biochar (APA-C500) is 11 m^2/g indicating that the surface area of biochar increased by 31.71% after pyrolysis. Surface area and pore volume typically increase with temperature as more volatile compounds are released from the biomass, despite the compromise of a lower biochar output [25]. In a study by Lee *et al.* [26], a calcium oxide-based catalyst with a surface area of 0.07 m^2/g derived from waste obtuse horn shell was successfully used in the transesterification of palm oil to biodiesel with an optimum palm oil conversion of 86.75%. The catalyst was thermally activated at 800 ºC for 3 h. The decreased surface area (0.07 m^2/g) was caused by the agglomeration of microscopic crystals as a result of employing the high calcination temperature (800 ºC). In another study by Hu *et al.* [27], waste freshwater mussel shell (FMS) catalyst with a surface area of 23.2 m^2/g was successfully utilised in the transesterification of Chinese tallow oil with a biodiesel yield above 90%. Surface area of *A. pinnata* biochar is comparable to other

TABLE-1
MOISTURE CONTENT AND LOSS ON IGNITION DATA OF UNCALCINED *A. pinnata* SAMPLE (APA-C0)

Physical property	Initial weight (W_i) (g)	Temperature (ºC)	Time (h)	Final weight (W_f) (g)	Difference in weight ($\Delta W = W_i - W_f$) (g)	Percentage ($\Delta W/W_i$) × 100
Moisture content (M)	0.5011	110	2	0.4230	0.0781	15.58
Loss on ignition (LOI)	0.2047	750	1	0.1031	0.1016	49.63

TABLE-2
ASH CONTENT DATA OF UNCALCINED *A. pinnata* SAMPLE (APA-C0)

Physical property	Initial weight (w_i) (g)	Temperature (ºC)	Time (h)	Final weight (w_f) (g)	(w_f/w_i)	Percentage (w_f/w_i) × 100
Ash content (A)	0.2047	750	1	0.1031	0.5036	50.36

TABLE-3
BET SURFACE AREA, PORE VOLUME AND PORE SIZE VALUES OF UNCALCINED AND CALCINED *A. pinnata* BIOCHAR SAMPLES

Sample type	BET surface area (m^2/g)	Micropore volume (cm^3/g)	Pore size (nm)
APA-C0	8.5424	0.0077	16.25
APA-C500	11.252	0.0078	13.84

biomass-based catalyst used in transesterification reaction thus making it a suitable candidate for catalytic application.

Thermal studies: To observe the thermal stability of *A. pinnata* biomass thermogravimetric analysis (TGA) of the uncalcined sample (APA-C0) was carried out at a range of temperature of 0-700 ºC with a slow heating rate of 10 ºC/min in a nitrogen environment. The TGA curve (Fig. 2) shows three stages of weight loss for the biomass. The first stage (25-220 ºC) exhibits a minor weight loss of 2.4%, attributed to the removal of adsorbed moisture and represents the drying phase [28]. The second stage (220-500 ºC) corresponds to the main pyrolysis region, where decomposition of lipids, proteins and carbohydrates occurs, resulting in the amorphous char formation, with a weight loss of 3.76%. The third stage (500-700 ºC) represents the carbonisation region, involving decomposition of carbonates and evolution of CO and CO_2, showing the highest weight loss of 23%. The final residue was about 70% of the initial mass, indicating significant inorganic content in the biomass [29]. Temperatures between 500 and 700 ºC were considered suitable for biochar production, as they promote carbonisation while maintaining yield. At higher temperatures, gasification and pore widening may occur, reducing microporosity and biochar yield, and the resulting chars are generally poorly crystalline in nature [24,30,31].

FT-IR spectral studies: The FT-IR spectrum of uncalcined *A. pinnata* biochar (APA-C0) shown in Fig. 3a as well as that of calcined in a muffle furnace at 500 ºC (APA-C500) shown in Fig. 3b shows a strong broad band 3750 cm^{-1}, which is attributed to Si-OH stretching vibration [32,33]. The broad band at 3495 cm^{-1} in both APA-C0 and APA-C500 is attributed to O-H stretching vibration of alcoholic OH groups

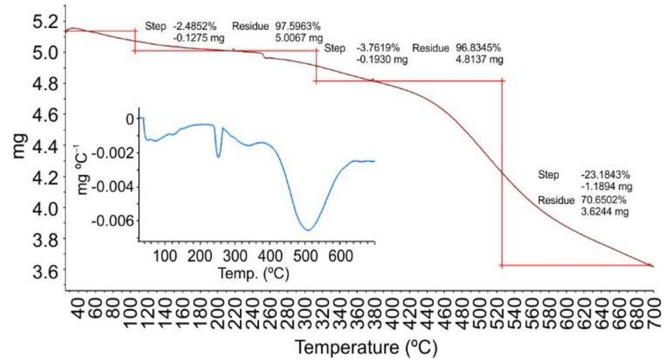

Fig. 2. TGA plots of uncalcined *Azolla pinnata* biochar (APA-C0)

[34] as well as to N-H stretching mode of amides [32]. The broad band indicates the presence of hydrogen bonding, which decreases somewhat in the calcined sample. The peaks beyond 3300-3100 cm^{-1} region in the APA-C0 spectrum corresponds to O-H stretching vibration of adsorbed water molecules on the surface of the catalyst, which becomes narrower under the influence of thermal treatment as evident from the APA-C500 spectrum. The peaks beyond 2962-2605 cm^{-1} region are assigned to organic groups such as methyl and methylene groups in fatty acids some of which disappear after pyrolysis as evident from the (APA-C500) spectrum [35,36]. The strong peaks located at 1601 is assigned to C=O stretching (protein amide-I) and the bands at 1200-950 cm^{-1} characterised the C–O–C stretching vibration absorption of polysaccharide [37].

The strong peaks located at 1105 cm^{-1} and 451 cm^{-1} are attributed to the Si-O-Si stretching band and Si–O–Si deformation vibrations of SiO_2, which is consistent with the results reported by Betiku *et al.* [34]. The presence for carbonates (CO_3^{2-}) in the form of calcite ($CaCO_3$) in the ash is evident from the peaks at 1423 cm^{-1} that corresponds to C-O stretching of CO_3^{2-} while the peak at 883 cm^{-1} corresponds to CO_3^{2-} bending. The strong peaks at 729 cm^{-1} and 451 cm^{-1} were assigned for Ca-O vibration [38]. The band at 1384 cm^{-1} (asym. stretching) and 1105 cm^{-1} (sym. stretching) and the moderate peak at 619 cm^{-1} (asym. bending) are attributed to SO_4^{2-} groups [39]. It can be seen that there is not much difference in the two

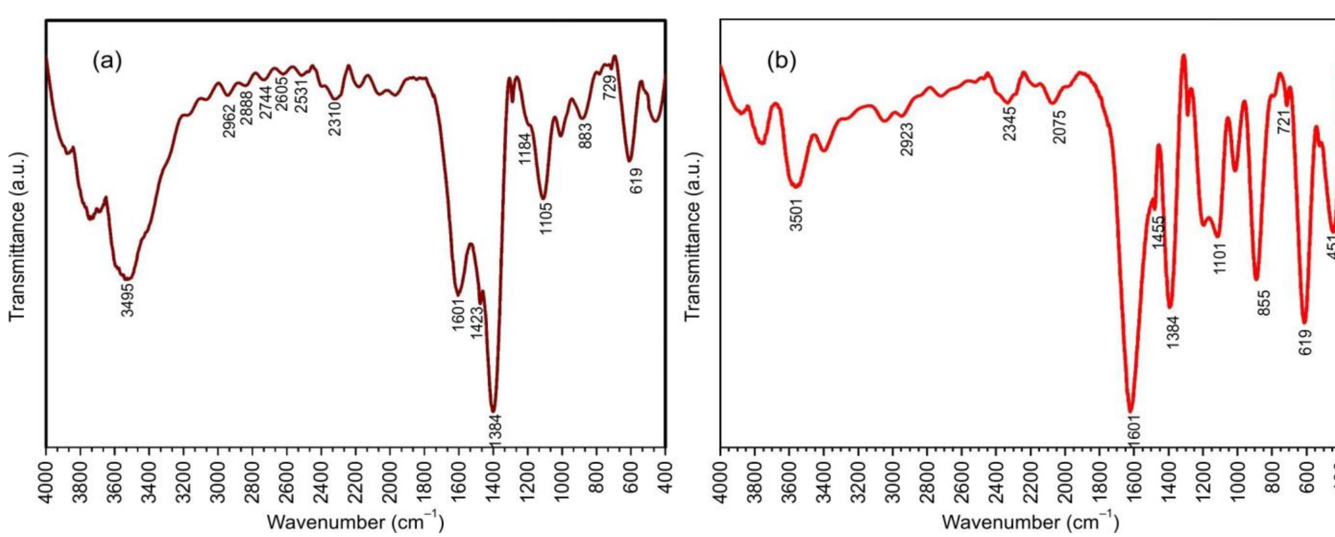

Fig. 3. FT-IR spectra of (a) uncalcined *Azolla pinnata* biochar (APA-C0) and (b) calcined *Azolla pinnata* biochar (APA-C500)

spectra obtained except for the disappearance of the peaks from 3000 cm^{-1} to 2864 cm^{-1}, which indicates the loss of volatile organic groups such as alkane, alkene, alkyne and aldehydic groups present in the calcined *A. pinnata* biochar (APA-C500) in the C500 spectra.

FESEM studies: The surface morphology and composition of the uncalcined *A. pinnata* biochar (APA-C0) and the calcined *A. pinnata* biochar (APA-C500) were analysed by FESEM and EDX. Uncalcined APA-C0 shows nonporous and irregular structures (Fig. 4). On calcination at 500 ºC the crystallinity of the particles increases which is evident from the FESEM images of the calcined ash (APA-C500) (Fig. 5).

Calcined *A. pinnata* biomass undergoes the surface alteration, transitioning from smooth and flat to a mix of smaller aggregates and polycrystalline surfaces after 3 h of calcination at 500 ºC. The subsequent microstructure shows that the surface area increased from 8 to 11 m^2/g as a result of calcination, which may enhance its catalytic activity.

Various nanoparticles were observed in APA-C0 with agglomerated and irregular morphologies, including rhombohedral (159-372 nm), hexagonal (152-257 nm), sheet- or needle-like (~370 nm) and spherical particles (12-52 nm), which became more prominent after calcination (APA-C500). At higher magnification, loosely packed agglomerates composed of fine particles were visible, indicating polycrystalline nature. The spherical particles are attributed to CaO nanoparticles, while rhombohedral and needle-like structures correspond to calcite and aragonite phases of $CaCO_3$, consistent with previous reports [38,40-42].

EDX studies: To investigate the elemental composition of biomass, EDX analyses were also carried out on APA-C0 and APA-C500 (Fig. 6). EDX analyses confirm the presence of carbon, silicon, oxygen, sodium, magnesium, calcium, potassium and chlorine as the major elements whereas phosphorus, sulfur, iron, manganese, aluminum and nitrogen are present in trace amounts. These results are in-agreement with the FT-IR spectra and PXRD results.

PXRD studies: The PXRD pattern of uncalcined *A. pinnata* biochar (APA-C0) is depicted in Fig. 7. Sharp peaks indicate the presence of crystalline phases in powder X-ray diffraction experiments. It is evident from the PXRD data that nanocrystalline phases are present in the *A. pinnata* ash which is further confirmed from FESEM analysis. The investigation confirmed the existence of inorganic component combinations.

As evident from the analysis, potassium was one of the key components of the biochar, which was found in the form

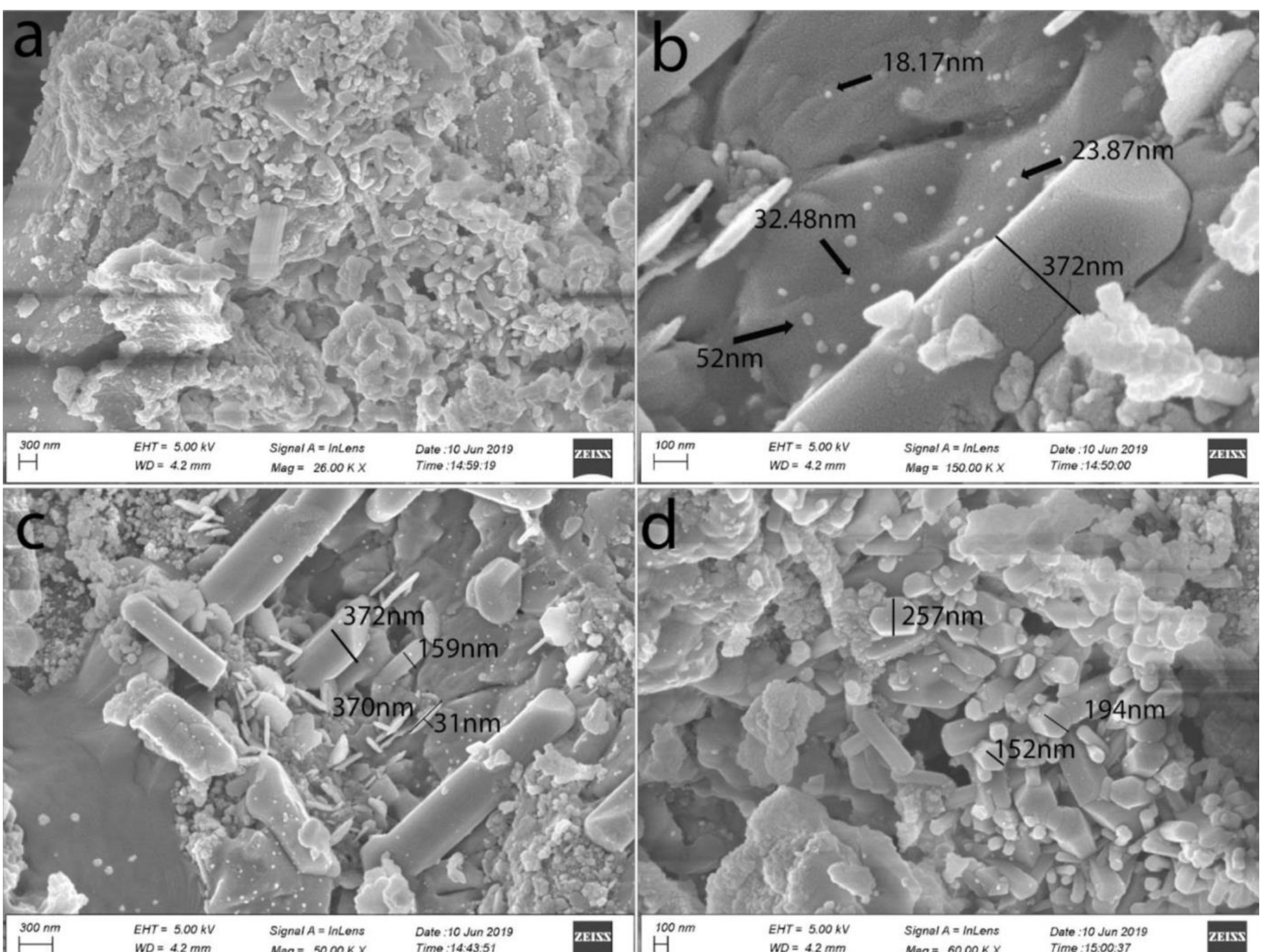

Fig. 4. FESEM images of the uncalcined *Azolla pinnata* biochar (APA-C0)

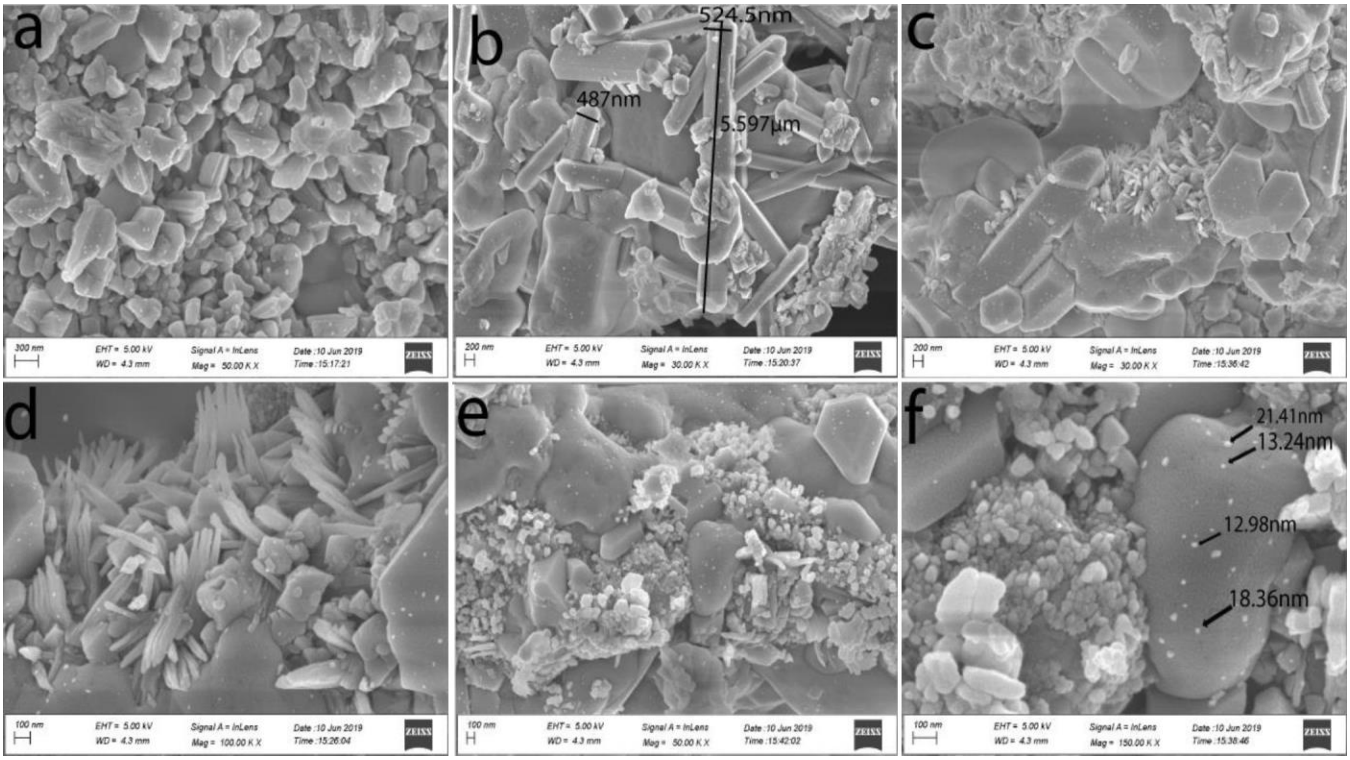

Fig. 5. FESEM images of the calcined *Azolla pinnata* biochar (APA-C500)

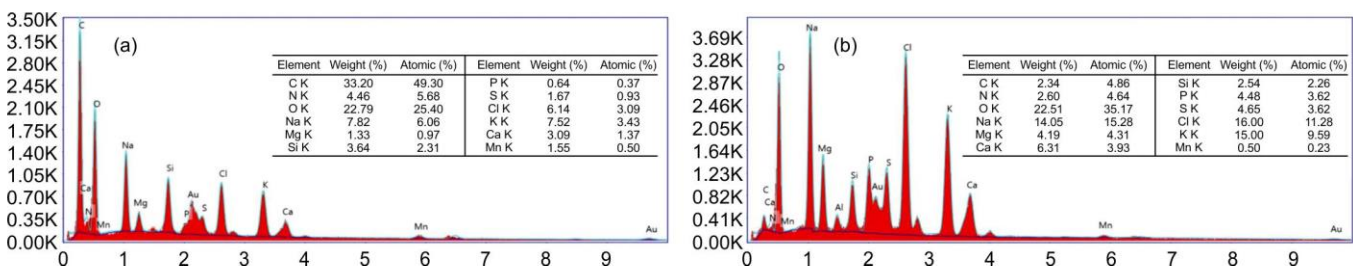

Fig. 6. EDX spectra of (a) uncalcined *Azolla pinnata* biochar (APA-C0) and (b) calcined *Azolla pinnata* biochar (APA-C500)

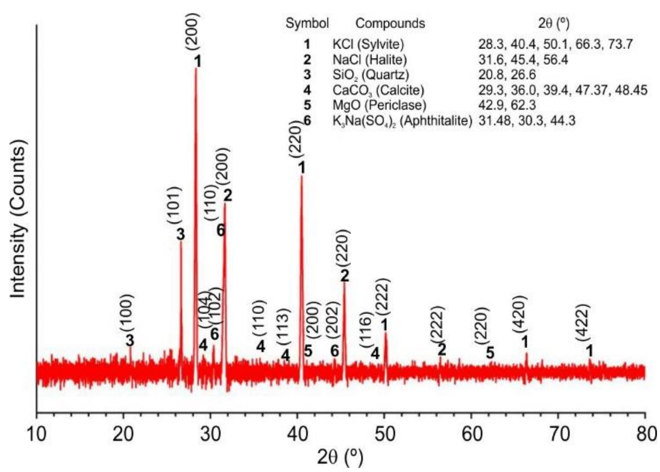

Fig. 7. PXRD spectrum of uncalcined *Azolla pinnata* biochar (APA-C0)

of KCl (sylvite). Comparison of the PXRD pattern with JCPDS data confirmed the presence of multiple crystalline phases in APA-C0. High-intensity peaks at 2θ values of 28.34º and 40.52º, along with peaks at 50.19º, 58.81º, 66.39º and 73.71º (JCPDS card no. 41-1476), correspond to KCl, indicating significant potassium content. Peaks at 27.18º, 31.62º, 45.40º, 56.42º and 75.19º (JCPDS 00-05-0628) confirm NaCl (halite). Strong reflections at 26.64º and 20.85º, with additional peaks at 36.54º, 39.46º, 42.45º and 50.10º (JCPDS 01-083-0539), indicate crystalline SiO_2 (quartz), also supported by FESEM observations. Further peaks at 29.3º, 36.0º, 39.4º, 47.3º and 48.4º (JCPDS 05-0586) correspond to $CaCO_3$ (calcite), while reflections at 42.9º, 62.3º and 78.6° (JCPDS 87-0653) confirm MgO. Minor phases such as $CaSO_4$ (25.4º and 31.3°, JCPDS 00-037-1496) and aphthitalite $K_3Na(SO_4)_2$ (30.3º, 31.48º and 44.3°, JCPDS 00-20-0928) were also detected, indicating the presence of alkali and alkaline earth mineral components in the biochar.

XRF studies: XRF analysis confirmed SiO_2, CaO and MgO as major oxides in APA-C0 (Table-4). The biochar exhibited basic nature (pH 10.54), good thermal stability up to 500 ºC and moderate surface area with mesoporous characteristics. Spectroscopic and chemical analyses indicated that the material mainly consists of oxides of Ca, Mg and Si, along with chlorides of K and Na, while sulfates and phosphates of elements such as Na, K, Ca, Mg, Si and Fe were present in trace amounts, consistent with PXRD results. PXRD identified KCl, NaCl and SiO_2 as dominant phases with moderate MgO and

TABLE-4
QUANTITATIVE XRF CHEMICAL ANALYSIS DATA OF UNCALCINED *Azolla pinnata* BIOCHAR APA-C0

Major oxides	Weight (%)
SiO_2	15.19
CaO	5.79
MgO	5.70

$CaCO_3$, whereas EDX confirmed K, Na, Cl, Si, C and O as major elements and Ca and Mg in moderate quantities. Calcination at 500 ºC increased the surface area of APA-C0 by 31.71% and FESEM images revealed hexagonal crystalline structures with enhanced surface roughness after heating. The presence of CaO and $CaCO_3$ is particularly significant, as CaO is a well-known heterogeneous base catalyst due to its high basicity and low toxicity. Biomass-derived CaO materials have been widely explored as sustainable catalysts, especially for transesterification reactions. Therefore, *A. pinnata* biochar containing CaO and $CaCO_3$ shows potential as a low-cost, eco-friendly heterogeneous base catalyst for future catalytic applications.

Conclusion

The biochar produced from sun-dried *Azolla pinnata* is thermally stable and composed mainly of oxides of Ca, Mg and Si, along with chlorides of K and Na, while sulfates and phosphates of elements such as Na, K, Ca, Mg, Si, Fe and Al are present in trace amounts. PXRD analysis identified KCl, NaCl and SiO_2 as major phases with moderate amounts of MgO and $CaCO_3$. These characteristics are comparable to Ca-rich biomass-derived materials used as heterogeneous base catalysts, indicating its potential for catalytic applications. In addition, the presence of nutrients such as Ca, Mg, N, P and K suggests possible use as a soil amendment or natural fertilizer, particularly for acidic soils. Utilization of *A. pinnata* biomass also offers a sustainable and cost-effective approach to manage its excessive growth while supporting future studies on catalytic performance and agricultural applications.

ACKNOWLEDGEMENTS

The authors acknowledge the Department of Chemistry, Gauhati University for allowing us to investigate the sample through FTIR, PXRD, TGA, BET, FESEM, EDX and XRF spectral analysis.

CONFLICT OF INTEREST

The authors declare that there is no conflict of interests regarding the publication of this article.

DECLARATION OF AI-ASSISTED TECHNOLOGIES

During the preparation of this manuscript, the authors used an AI-assisted tool(s) to improve the language. The authors reviewed and edited the content and take full responsibility for the published work.

REFERENCES

1. G.A. Peters, *Arch. Microbiol.*, **103**, 113 (1975); https://doi.org/10.1007/BF00436337
2. G.A. Peters, *Bioscience*, **28**, 580 (1978); https://doi.org/10.2307/1307514
3. T.A. Lumpkin and D.L. Plucknett, *Econ. Bot.*, **34**, 111 (1980); https://doi.org/10.1007/BF02858627
4. A. Hussner, I. Stiers, M.J.J.M. Verhofstad, E.S. Bakker, B.M.C. Grutters, J. Haury, J.L.C.H. van Valkenburg, G. Brundu, J. Newman, J.S. Clayton, L.W.J. Anderson and D. Hofstra, *Aquat. Bot.*, **136**, 112 (2017); https://doi.org/10.1016/j.aquabot.2016.08.002
5. A. Arora and S. Saxena, *Biomass Bioenergy*, **29**, 60 (2005); https://doi.org/10.1016/j.biombioe.2005.02.002
6. N. Muradov, M. Taha, A.F. Miranda, K. Kadali, A. Gujar, S. Rochfort, T. Stevenson, A.S. Ball and A. Mouradov, *Biotechnol. Biofuels*, **7**, 30 (2014); https://doi.org/10.1186/1754-6834-7-30
7. A. Sood, P.L. Uniyal, R. Prasanna and A.S. Ahluwalia, *Ambio*, **41**, 122 (2012); https://doi.org/10.1007/s13280-011-0159-z
8. B. Kollah, A.K. Patra and S.R. Mohanty, *Environ. Sci. Pollut. Res.*, **23**, 4358 (2016); https://doi.org/10.1007/s11356-015-5857-9
9. H.Z. Hamdan and A.F. Houri, *Environ. Sci. Pollut. Res.*, **29**, 16912 (2022); https://doi.org/10.1007/s11356-021-16986-6
10. R.J.E. Vroom, A.J.P. Smolders, B.P. Van de Riet, L.P.M. Lamers, E. Güngör, S. Krosse, G.M. Verheggen-Kleinheerenbrink, N.R. Van der Wal and S. Kosten, *Water Res.*, **254**, 121411 (2024); https://doi.org/10.1016/j.watres.2024.121411
11. O.A. Alalade and E.A. Iyayi, *Int. J. Poult. Sci.*, **5**, 137 (2006).
12. N. Katayama, M. Yamashita, Y. Kishida, C.C. Liu, I. Watanabe, H. Wada, *Acta Astronaut.*, **63**, 1093 (2008); https://doi.org/10.1016/j.actaastro.2008.01.023
13. M. Wagner, *Bot. Rev.*, **63**, 1 (1997); https://doi.org/10.1007/BF02857915
14. M. Varkolu, S. Gundekari, Omvesh, V.C.S. Palla, S. Bhattacharjee, P. Kumar and T. Vinodkumar, *Catalysts*, **15**, 243 (2025); https://doi.org/10.3390/catal15030243
15. Y. Xie, L. Wang, H. Li, L.J. Westholm, L. Carvalho, E. Thorin, Z. Yu, X. Yu and Ø. Skreiberg, *J. Anal. Appl. Pyrol.*, **161**, 105405 (2022); https://doi.org/10.1016/j.jaap.2021.105405
16. J. Lehmann and S. Joseph, Biochar for Environmental Management, Science, Technology and Implementation, Routledge, edn. 2 (2015).
17. M. Ahmad, A.U. Rajapaksha, J.E. Lim, M. Zhang, N. Bolan, D. Mohan, M. Vithanage, S.S. Lee and Y.S. Ok, *Chemosphere*, **99**, 19 (2014); https://doi.org/10.1016/j.chemosphere.2013.10.071
18. C. Gallego-Ramírez, E. Chica and A. Rubio-Clemente, *J. Environ. Chem. Eng.*, **12**, 112425 (2024); https://doi.org/10.1016/j.jece.2024.112425
19. V.C. Srivastava, I.D. Mall and I.M. Mishra, *Colloids Surf. A: Physicochem. Eng. Asp.*, **312**, 172 (2008); https://doi.org/10.1016/j.colsurfa.2007.06.048
20. S.K. Manikandan, P. Pallavi, D. Bhattacharjee, D.A. Giannakoudakis, K. Shetty, I.A. Katsoyiannis and V. Nair, *Molecules*, **28**, 719 (2023); https://doi.org/10.3390/molecules28020719
21. Z. Zeng, A. Umeh, G.A. Iyengar, F. Qi and R. Naidu, *J. Environ. Chem. Eng.*, **12**, 114262 (2024); https://doi.org/10.1016/j.jece.2024.114262
22. R. Shan, J. Han, J. Gu, H. Yuan, B. Luo and Y. Chen, *Resour. Conserv. Recycl.*, **162**, 105036 (2020); https://doi.org/10.1016/j.resconrec.2020.105036
23. Z. Wei, C. Xu and B. Li, *Bioresour. Technol.*, **100**, 2883 (2009); https://doi.org/10.1016/j.biortech.2008.12.039
24. N. Nakatani, H. Takamori, K. Takeda and H. Sakugawa, *Bioresour. Technol.*, **100**, 1510 (2009); https://doi.org/10.1016/j.biortech.2008.09.007
25. X. Xiong, I.K.M. Yu, L. Cao, D.C.W. Tsang, S. Zhang and Y.S. Ok, *Bioresour. Technol.*, **246**, 254 (2017); https://doi.org/10.1016/j.biortech.2017.06.163
26. S.L. Lee, Y.C. Wong, Y.P. Tan and S.Y. Yew, *Energy Convers. Manag.*, **93**, 282 (2015); https://doi.org/10.1016/j.enconman.2014.12.067
27. S. Hu, Y. Wang and H. Han, *Biomass Bioenergy*, **35**, 3627 (2011); https://doi.org/10.1016/j.biombioe.2011.05.009
28. A. Agrawal and S. Chakraborty, *Bioresour. Technol.*, **128**, 72 (2013); https://doi.org/10.1016/j.biortech.2012.10.043

29. Q.V. Bach and W.H. Chen, *Bioresour. Technol.*, **246**, 88 (2017); https://doi.org/10.1016/j.biortech.2017.06.087
30. N. Muradov, B. Fidalgo, A.C. Gujar, N. Garceau and A. T-Raissi, *Biomass Bioenergy*, **42**, 123 (2012); https://doi.org/10.1016/j.biombioe.2012.03.003
31. M. Keiluweit, P.S. Nico, M.G. Johnson and M. Kleber, *Environ. Sci. Technol.*, **44**, 1247 (2010); https://doi.org/10.1021/es9031419
32. L.G. Benning, V.R. Phoenix, N. Yee and K.O. Konhauser, *Geochim. Cosmochim. Acta*, **68**, 743 (2004); https://doi.org/10.1016/S0016-7037(03)00488-5
33. E.A. Paukshtis, M.A. Yaranova, I.S. Batueva and B.S. Bal'zhinimaev, *Micropor. Mesopor. Mater*., **288**, 109582 (2019); https://doi.org/10.1016/j.micromeso.2019.109582
34. E. Betiku, A.O. Etim, O. Pereao and T.V. Ojumu, *Energy Fuels*, **31**, 6182 (2017); https://doi.org/10.1021/acs.energyfuels.7b00604
35. M.I. Bird, C.M. Wurster, P.H. de Paula Silva, A.M. Bass and R. de Nys, *Bioresour. Technol*., **102**, 1886 (2011); https://doi.org/10.1016/j.biortech.2010.07.106
36. J.N. Murdock and D.L. Wetzel, *Appl. Spectrosc. Rev*., **44**, 335 (2009); https://doi.org/10.1080/05704920902907440
37. T. Zhao, X. Han and H. Cao, *ACS Omega*, **5**, 33262 (2020); https://doi.org/10.1021/acsomega.0c04961
38. L. Habte, N. Shiferaw, D. Mulatu, T. Thenepalli, R. Chilakala and J.W. Ahn, *Sustainability*, **11**, 3196 (2019); https://doi.org/10.3390/su11113196
39. M.R. Soto-Vásquez, P.A.A. Alvarado-García, F.S. Youssef, M.L. Ashour, H.A. Bogari and S.S. Elhady, *Mar. Drugs*, **21**, 36 (2023); https://doi.org/10.3390/md21010036
40. Z. Mirghiasi, F. Bakhtiari, E. Darezereshki and E. Esmaeilzadeh, *J. Ind. Eng. Chem*., **20**, 113 (2014); https://doi.org/10.1016/j.jiec.2013.04.018
41. M.M.H. Al Omari, I.S. Rashid, N.A. Qinna, A.M. Jaber and A.A. Badwan, *Profiles Drug Subst. Excipients Relat. Methodol.*, **41**, 31 (2016); https://doi.org/10.1016/bs.podrm.2015.11.003
42. H. Wang, V. Alfredsson, J. Tropsch, R. Ettl and T. Nylander, *ACS Appl. Mater. Interfaces*, **5**, 4035 (2013); https://doi.org/10.1021/am401348v